Low-frequency excitation spectra in double-walled armchair carbon nanotubes

Y. H. Ho,* G. W. Ho, S. C. Chen, J. H. Ho,† and M. F. Lin‡
Department of Physics, National Cheng Kung University, Tainan 70101, Taiwan
(Received 4 June 2007; revised manuscript received 26 June 2007; published 17 September 2007)

The low-frequency electronic excitations of the double-walled armchair carbon nanotubes are investigated by the random-phase approximation. Both the intertube atomic hoppings and the intertube *e-e* interactions are included in the calculations simultaneously. The intertube atomic hoppings significantly alter the low-energy bands and thus enrich the low-frequency excitation spectra. There are more single-particle excitation channels and plasmon modes. These excitations strongly depend on the symmetric configurations of the double-walled system and the transferred momentum, such as the number, the existence, the strength, and the frequency of plasmon modes.

DOI: 10.1103/PhysRevB.76.115422 PACS number(s): 73.63.Fg, 71.45.Gm, 73.20.Mf

Carbon nanotubes have attracted a lot of interesting theoretical and experimental studies since the discovery by Iijima in 1991.[1] Owing to the peculiar electronic and mechanical properties, carbon nanotubes are highly potential materials for nanoscaled electronic devices in the next generation.[2] Carbon nanotubes could exist in the single-walled forms (SWCNTs) and the multiwalled ones (MWCNTs).[1,3] Among them, the double-walled carbon nanotubes (DWCNTs) are the simplest ones in understanding the effects of the intertube atomic hoppings on electronic properties. DWCNTs are steadier than SWCNTs in terms of the thermal and chemical stabilities; they exhibit the greater rigidity supported by the van der Waals forces.[4,5] With the advancement of synthesis techniques, the high-purity DWCNTs could be produced.[6,7] Geometric structures (radius r and chiral angle θ) and electronic properties were determined by various experimental measurements.[8–15] SWCNTs are gapless metals or semiconductors depending on geometric structures.[13] A SWCNT is a rolled-up graphite sheet, the structure of which is thus fully specified by a two-dimensional lattice vector $\mathbf{R}_x = m\mathbf{a}_1 + n\mathbf{a}_2$, where $\mathbf{a}_1$ and $\mathbf{a}_2$ are primitive lattice vectors of a graphite sheet. The parameters (m,n), therefore, uniquely define a SWCNT. (m,m) and $(m,0)$ are, respectively, armchair and zigzag SWCNTs. All armchair (m,m) SWCNTs are metallic. In addition to r and θ, the low-energy electronic structure of DWCNTs is substantially influenced by the intertube atomic hoppings and the symmetric configurations.[16–20] Their main features would be directly reflected in the low-frequency Coulomb excitations.

The collective and single-particle excitations in SWCNTs have been extensively studied experimentally[21,22] and theoretically.[23,24] The π-band electrons, which are formed by the $2p_z$ orbitals, exhibit the $\sim 5-7$ eV π plasmon.[21,22] All metallic and narrow-gap semiconducting SWCNTs own the low-frequency plasmons with $\omega_p < 1$ eV.[25–28] These collective excitation modes mainly result from charge carriers in the low-energy bands near the Fermi level (E_F), and they belong to acoustic plasmons at finite temperature. The way the low-frequency plasmons survive in armchair DWCNTs would be investigated in detail.

As regards the excitation spectra of DWCNTs, most theoretical studies were based on the free electron gas model[29–33] or the simple π-band model without the intertube atomic hoppings.[25,26,34–36] These two kinds of models do not consider the effects of the intertube atomic hoppings on the low-energy bands and the Coulomb excitations. The previous studies[16–20] showed that the intertube atomic hoppings significantly affect the low-energy bands and the distribution of free carriers near E_F. Such carriers could tunnel between two different carbon nanotubes under the consideration of the intertube atomic hoppings. The DWCNTs are thus expected to exhibit rich single-particle and collective excitations.

The low-frequency excitation spectra of the armchair DWCNTs in the presence of the intertube atomic hoppings are investigated in this work. The low-energy electronic structure is evaluated by the tight-binding model. Within the random-phase approximation (RPA),[24] the intertube atomic hoppings and the intertube Coulomb excitations are taken into account in the calculations of excitation spectra simultaneously. They both dominate the *e-h* excitations and the plasmon modes. The intertube atomic hoppings enrich the carrier distribution and thus the excitation channels. The Coulomb excitation spectra strongly depend on the transferred momentum and the symmetric configurations, such as the dispersion relations, the existence, the strength, and the number of plasmons. The predicted results could be verified by the experimental measurements from the electron energy loss spetroscopy (EELS).

The (5,5)-(10,10) armchair DWCNT, with the commensurate graphene stacking, is chosen for a model study. There are three kinds of symmetric structures [C_5, D_{5h}, and S_5 in Figs. 1(b)–1(d)], according to the translational and rotational symmetries about the nanotube axis. A primitive unit cell consists of four and eight atoms from the inner and outer nanotubes, respectively. The π-electronic structure originates from the $2p_z$ orbitals normal to the nanotube surface. The DWCNTs own the intratube and intertube atomic hoppings in the tight-binding model. The former are confined to the nearest-neighbor interactions, and the latter account for the interatom distance on the projection surface shorter than the C-C bond length ($b = 1.42$ Å). The tight-binding Hamiltonian is given by

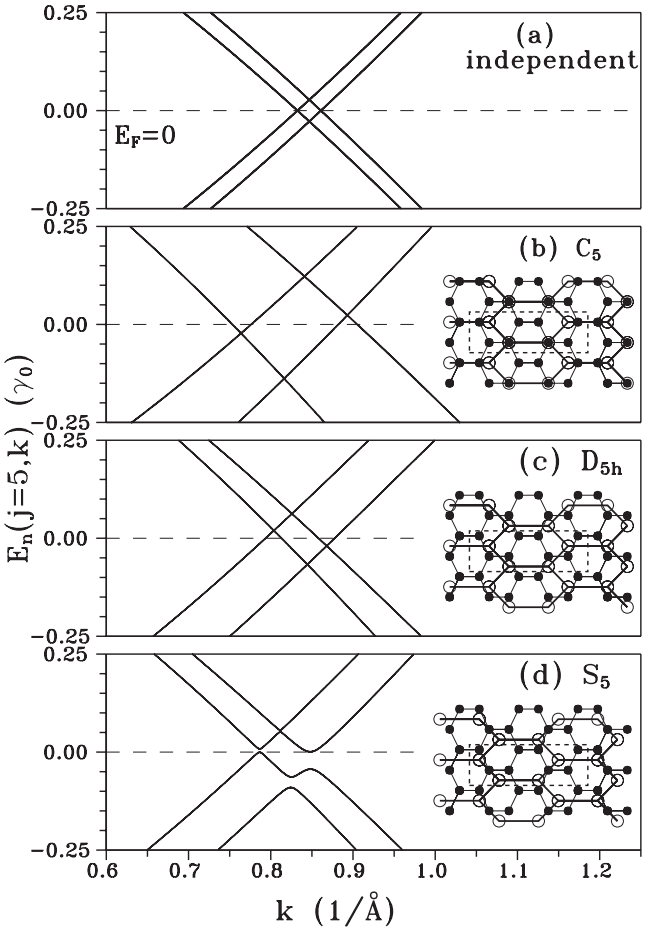

FIG. 1. The low-energy bands of the double-walled (5,5)-(10,10) carbon nanotubes for three symmetric configurations: (b) C_5, (c) D_{5h}, and (d) S_5. Also shown in (a) for comparison are those without the intertube atomic hoppings.

$$H = \gamma_0 \sum_{l=1}^{2} \sum_{i,i'} h(\theta_{l,i;l,i'}) c_{l,i'}^{\dagger} c_{l,i} - W \sum_{l \neq l'=1}^{2} \sum_{i,i'} h(\theta_{l,i;l',i'}) e^{a-d_{l,i;l',i'}/\delta} c_{l',i'}^{\dagger} c_{l,i}, \quad (1)$$

where $c_{l,i}$ ($c_{l,i}^{\dagger}$) is the creation (annihilation) operator for the ith atom on the lth nanotube. The first and second terms in Eq. (1), respectively, correspond to the intratube and intertube atomic hoppings. These two kinds of atomic hoppings contain the π bonding ($V_{pp\pi}$=−2.66 eV=γ_0) and the σ bonding ($V_{pp\sigma}$=6.38 eV). Moreover, the major intratube and intertube atomic hoppings are $V_{pp\pi}$ and $V_{pp\sigma}$, respectively. The curvature effect due to the misorientation of the $2p_z$ orbitals makes the atomic hopping integral $h(\theta_{l,i;l,i'})$ depend on the relative angle $\theta_{l,i;l,i'}$ between two orbitals. Also note that the increase of the interatom distance ($d_{l,i';l',i'}$) leads to the rapid decrease of the intertube atomic hoppings in the exponential form. Parameters W=1/8 and δ=0.45 Å are obtained from the comparison with the first-principles calculations and the experimental data.[16,37,38] By diagonalizing the

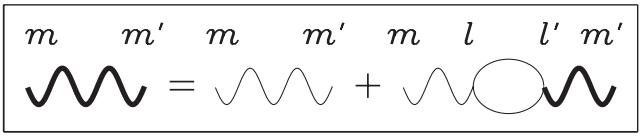

FIG. 2. The Feynman diagram of the effective Coulomb potential within the RPA.

12×12 Hamiltonian, we obtain state energy $E_n(j,k)$ and wave function $\psi_n(j,k)=\Sigma_{li} u_{n,l,i}(j,k) a_{l,i}$, with the subband index n, the quantized angular momentum j, and the longitudinal wave vector k. The Bloch function is the superposition of 12 tight-binding functions $a_{l,i}$'s.

The π-electronic structure, without the intertube atomic hoppings, exhibits two pairs of linear subbands intersecting at E_F=0, as shown in Fig. 1(a). The left- and right-hand linear bands, respectively, correspond to the (5,5) and (10,10) nanotubes. The occupied valence bands are symmetric to the unoccupied conduction bands about E_F. Figures 1(b)–1(d) show the effects of the intertube atomic hoppings and the symmetric configurations on band structures. The symmetry between valence and conduction bands is absent. Energy dispersion relations in C_5 and D_{5h} systems remain linear, while the intertube atomic hoppings affect the dependence on the wave vector and the Fermi momenta (k_F's). The S_5 system owns the parabolic bands with several band-edge states. Both C_5 and D_{5h} systems are gapless metals, while the S_5 system is a narrow-gap semiconductor with $E_g \sim 3.2$ meV. Apparently, the intertube atomic hoppings in three systems have changed the excitation energies and the carrier distribution. Each Bloch function comes from the superposition of the tight-binding functions on the inner and outer nanotubes. The hybridization of these functions is strong near k_F's since the low-energy bands are significantly affected by the intertube atomic hoppings. The carrier tunneling between two different nanotubes is deduced to play an important role in the excitation spectra.

When the DWCNTs are perturbed by the time-dependent Coulomb potential $V_{mm'}^{ex}(q,L)$, their π electrons would screen the external field by the dynamic e-e interactions. The momentum transfer q and the angular momentum transfer L are conserved during the Coulomb interactions. The effective Coulomb potential between two electrons on the mth and m'th nanotubes within the RPA, as shown in Fig. 2, is characterized by the Dyson equation,

$$\epsilon_0 V_{mm'}^{eff}(q,L;\omega) = V_{mm'}^{ex}(q,L) + V_{mm'}^{in}(q,L;\omega) = V_{mm'}^{ex}(q,L) + \sum_{m,m'=1}^{2} V_{ml}^{ex}(q,L) P_{ll'}^{(1)}(q,L;\omega) V_{l'm'}^{eff}(q,L;\omega). \quad (2)$$

ϵ_0=2.4 is the background dielectric constant.[23–25,34] The effective Coulomb potential is the sum of the external and induced Coulomb potentials. The former $V_{mm'}^{ex}(q,L) = 4\pi e^2 I_L(qr_<) K_L(qr_>)/\epsilon_0$ is the bare intratube ($r_<=r_>$) or

intertube ($r_< \neq r_>$) Coulumb interaction. I_L (K_L) is the modified Bessel function of the first (second) kind of order L and $r_<$ ($r_>$) is the smaller (larger) nanotube radius. The latter $V^{in}_{mm'}(q,L;\omega)$ stems from the induced charges on two nanotubes. The screening charge density is the product of the bare response function and the effective Coulomb potential. $P^{(1)}_{ll'} \times(q,L;\omega)$, the RPA bubble in Fig. 2, is given by

$$P^{(1)}_{ll'}(q,L;\omega) = 2\sum_k \sum_{n,n'} \left[\sum_i u_{nli}(j,k) u^*_{n'l'i}(j+L,k+q) \right] \times \left[\sum_{i'} u^*_{nl'i'}(j,k) u_{n'l'i'}(j+L,k+q) \right] \times \frac{f[E_n(j,k)] - f[E_{n'}(j+L,k+q)]}{\omega_{nn'}(j,k;j+L,k+q) + \hbar\omega + i\Gamma}. \quad (3)$$

$f[E_n(j,k)]$ is the Fermi-Dirac distribution function. $\omega_{nn'}(j,k;j+L,k+q)=E_{n'}(j+L,k+q)-E_n(j,k)$ is excitation energy between the initial and final states. Γ is the energy width due to various deexcitation mechanisms. Both intratube polarizations ($P^{(1)}_{11}$ and $P^{(1)}_{22}$) and intertube polarizations ($P^{(1)}_{12}=P^{(1)}_{21}$) make contributions to the dynamic charge screening. They, respectively, correspond to the excited electrons and holes that are located on the same and different nanotubes. The intertube polarizations would vanish when the intertube atomic hoppings are neglected.

The effective Coulomb potential in Eq. (2) is associated with the loss spectrum which represents the intrinsic excitation properties. The probing electrons would transfer momentum, angular momentum, and energy (q,L,ω) to the armchair DWCNTs. Their distribution is assumed to be uniform on two nanotubes. The inelastic scattering probability, which is obtained from the detailed calculations within the Born approximation, is used to define the dimensionless loss function,[39]

$$\mathrm{Im}\left[\frac{-1}{\epsilon}\right] \equiv \frac{\sum_m \mathrm{Im}[-V^{eff}_{mm}(q,L;\omega)]}{\sum_{mm'} V^{ex}_{mm'}(q,L)/2}. \quad (4)$$

The denominator is the average value of the external Coulomb potentials on two nanotubes. The loss function or the screened response function in Eq. (4) is useful in understanding the collective excitations of the low-energy π electrons.

Only the low-frequency excitation spectra of the $L=0$ mode at zero temperature are discussed in this work. They result from the two pairs of conduction and valence bands nearest to the Fermi level (Fig. 1). The bare response functions directly reflect the main characteristics of the single-particle excitations between occupied and unoccupied states. Their imaginary parts represent the strength of the e-h pairs. $\mathrm{Im}[P^{(1)}_{11}]$, the intratube response function due to the excited electrons and holes on the inner nanotube, could exhibit the special singular structures, which is illustrated in Figs. 3(a)–3(d) with the four systems at $q=0.05$ Å and $\Gamma \to 0$ by the dashed curves. These structures are understood from the joint density of states $J_D(q,\omega)$ since $\mathrm{Im}[P^{(1)}_{11}]$ in Eq. (3) is proportional to it. $J_D(q,\omega)$, defined as $|\partial\omega_{nn'}(j,k;j,k+q)/\partial k|^{-1}_{\omega_{nn'}=\omega}$, is mainly determined by the energy dispersion relations and the critical points in the energy-wave-vector space. For the independent system, the linear energy dispersions [the left-hand two linear bands in Fig. 1(a)] and the Fermi-momentum states (the critical points) induce two finite discontinuities at $\omega \sim 1.5bq\gamma_0$. These two structures are close to each other since the difference in the slopes of the two linear bands is inapparent. With the use of the Kramers-Kronig relations, the real part $\mathrm{Re}[P^{(1)}_{11}]$ exhibits the singular logarithmic structures. Also notice that the finite discontinuities, the logarithmic divergences, and the square-root divergences would become the peak structures in the inclusion of the broadening effect (a finite Γ, not shown). The similar special structures are also found in the C_5 and D_{5h} systems with linear energy bands [Figs. 1(b) and 1(c)]. However, there are more singular structures at $\omega \sim 1.5bq\gamma_0$, and some extra singular structures with weak strength would occur at higher or lower frequencies [Figs. 3(b) and 3(c)]. The strong hybridization of the inner and outer tight-binding functions leads to more complicated excitation channels among all energy bands which explains the drastic changes in $P^{(1)}_{11}$. As to the narrow-gap S_5 system, the critical points are the band-edge states, but not the Fermi-momentum states. The excitation energies related to them have the parabolic or linear dependence on the wave vector. The parabolic bands could produce the square-root singular structures in $\mathrm{Im}[P^{(1)}_{11}]$ and $\mathrm{Re}[P^{(1)}_{11}]$. Apparently, the main features of the bare response functions are drastically changed by the different intertube atomic hoppings, e.g., the strength, the number, and the frequencies of the singular structures in $P^{(1)}_{11}$. The other bare response functions, $P^{(1)}_{22}$ and $P^{(1)}_{12}$ [Figs. 3(e) and 3(f) for the D_{5h} system], behave as $P^{(1)}_{11}$ [Fig. 3(c)], mainly owing to the intertube atomic hoppings. The only difference is the weaker strength in the intertube e-h excitations, $P^{(1)}_{12}$.

The screened response function is useful in understanding the low-frequency collective excitations and the measured spectra from EELS. The loss spectra of the independent system are shown in Fig. 4(a) for various q's. There are two clear peaks, and each peak corresponds to the collective excitations of charge carriers on two nanotubes. The intertube Coulomb interactions would make charge fluctuations on two nanotubes couple each other; therefore, the plasmon strength at the higher frequency is much stronger than that at the lower frequency. The intertube atomic hoppings bring about more complicated collective excitations, as shown in Figs. 4(b)–4(d). That the π electrons could be excited between any two energy bands is the main reason. The loss spectra exhibit more plasmon peaks (three, four, or five plasmon modes), while their intensities are reduced by the rich single-particle excitations. Each plasmon mode is associated with a specific excitation channel from the critical point. Some plasmon modes might disappear in the increasing of momentum because of the strong Landau damping. The

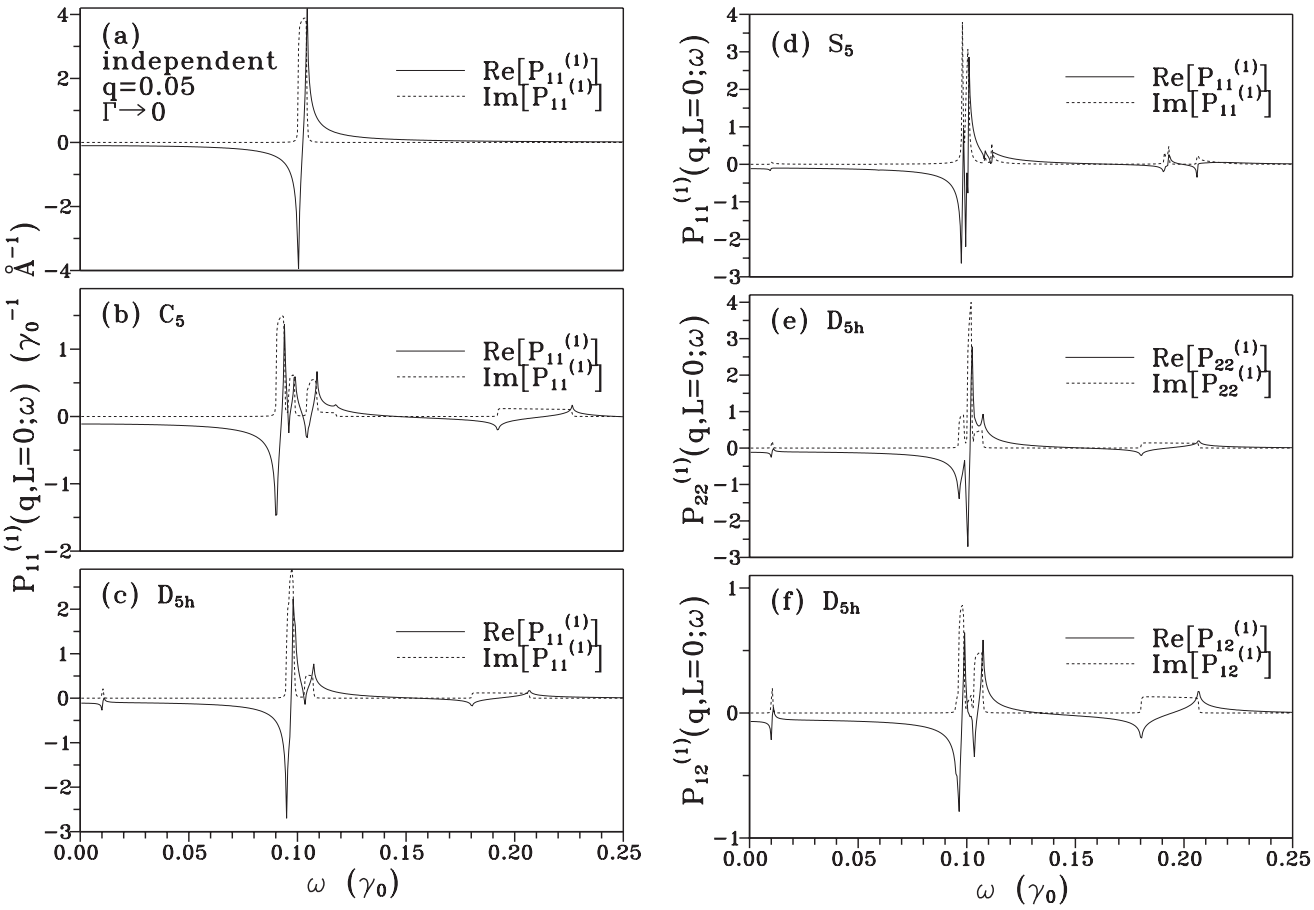

FIG. 3. The real and the imaginary parts of the bare response functions at $q=0.05$ Å^{-1}, $L=0$, and $\Gamma\rightarrow 0$ for (a) $P_{11}^{(1)}$ of the independent system, (b) $P_{11}^{(1)}$ of the C_5 system, (c) $P_{11}^{(1)}$ of the D_{5h} system, (d) $P_{11}^{(1)}$ of the S_5 system, (e) $P_{22}^{(1)}$ of the D_{5h} system, and (f) $P_{12}^{(1)}$ of the D_{5h} system.

most-energetic plasmons in the D_{5h} and S_5 systems own the strongest spectra, as it could be seen in the independent system. However, a simple relation between the frequency and the strength is absent in three kinds of symmetric configurations. The important differences among these systems in the screened response functions indicate that the experimental measurements from EELS could be utilized to identify the geometric structures.

The transferred momentum dominates the main features of the low-frequency plasmons. The plasmon frequencies ω_p's strongly rely on q, as shown in Figs. 5(a)–5(d). This result directly responds to the important characteristic of the low-energy bands, the strong dependence on the wave vector. Plasmons are quanta of the collective electron density oscillations. The dispersion relation with the transferred momentum means that the plasma oscillation of the two-coupled nanotubes behaves as a propagating wave, with wavelength $2\pi/q$ and group velocity $\partial\omega_p(q)/\partial q$. Plasmon is an acoustic (optical) mode, when its frequency vanishes (maintain a finite value) at the long wavelength limit $q\rightarrow 0$. There exist only two acoustic plasmons in the independent systems, and they could survive at large q's [Fig. 5(a)]. The intertube atomic hoppings drastically change the acoustic plasmons and create several optical plasmons. The C_5, D_{5h}, and S_5 systems, respectively, have two acoustic plasmons, one acoustic plasmon, and no acoustic plasmons. The former are completely suppressed by the serious *e-h* damping for q higher than the critical momentum (q_c). The absence of acoustic plasmon in the S_5 system lies in the narrow-gap characteristic. Most plasmons in three symmetric systems belong to optical modes. That the single-particle excitation energies about the critical points have finite values is the main reason. The main features of plasmons are determined by the energy gap, the critical points, and the wave-vector dependence of the low-energy bands. The symmetric configurations can be distinguished by the number, the frequency, and the momentum dependence of the plasmon modes.

In summary, the low-frequency electronic excitations of the double-walled armchair carbon nanotubes are studied within the linear RPA. This work could be further generalized to the multiwalled carbon nanotubes with more layers. The intertube atomic hoppings and the intertube Coulomb interactions are taken into account simultaneously. The former significantly affect the low-energy bands and thus enrich the excitation spectra. The wave-vector dependence, the critical points, and the energy gap of energy bands dominate the main characteristics of the bare and screened response functions. The intertube atomic hoppings induce more single-particle excitation channels and plasmon modes.

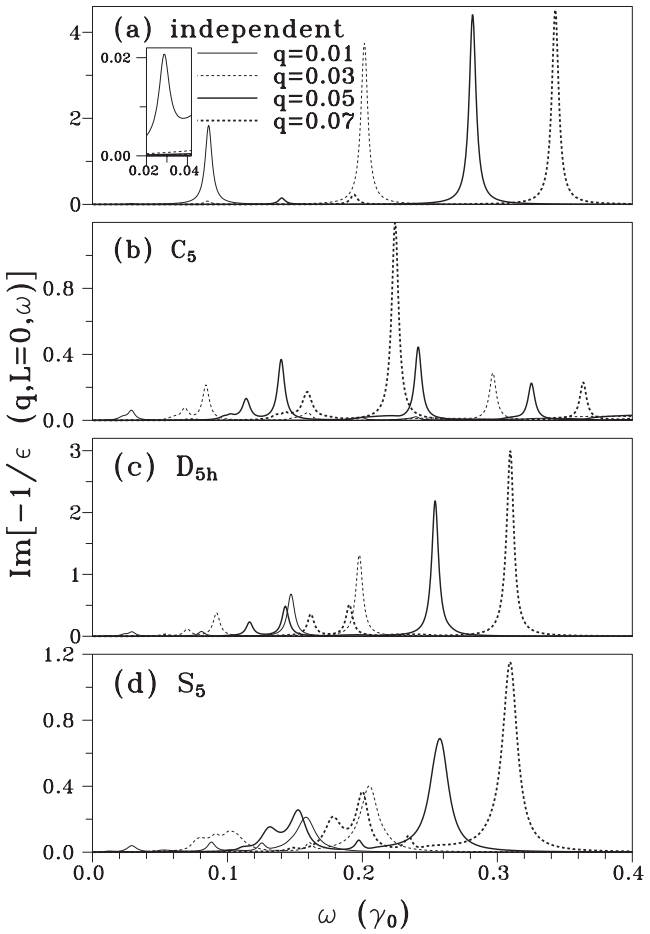

FIG. 4. The loss functions at various q's, $L=0$, and $\Gamma=3\times10^{-3}$ γ_0 for the four systems: (a) independent, (b) C_5, (c) D_{5h}, and (d) S_5.

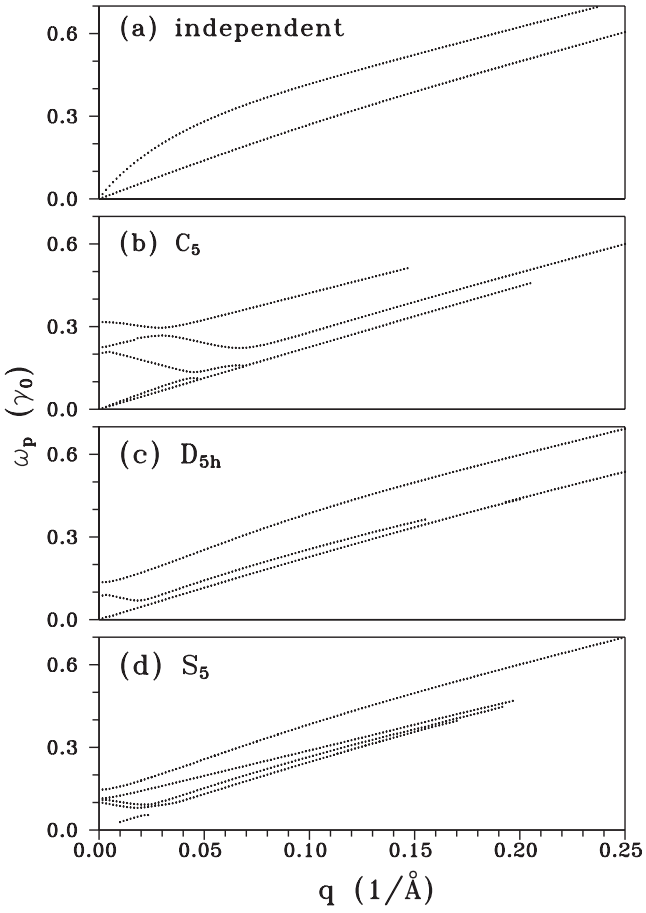

FIG. 5. The momentum-dependent plasmon frequencies for the (a) independent, (b) C_5, (c) D_{5h}, and (d) S_5 systems.

The *e-h* excitations exhibit the singular structures in the unscreened response functions, mainly owing to the Fermi-momentum states or the band-edge states. The plasmon strength is reduced by the intertube carrier tunneling. The number, the frequency, the strength, and the momentum dependence of plasmon modes strongly rely on the symmetric configurations. Most plasmons belong to optical modes, but not acoustic modes. The experimental measurements of EELS are predicted to be useful in determining the double-walled geometric structures.

This work was supported by the NSC and NCTS of Taiwan, under Grant No. NSC 95-2112-M-006-028-MY3.

*l2893104@mail.ncku.edu.tw
†jonhsu.ho@hotmail.com
‡mflin@mail.ncku.edu.tw

[1] S. Iijima, Nature (London) **354**, 56 (1991).
[2] R. H. Baughman, A. A. Zakhidov, and W. A. d. Heer, Science **297**, 787 (2002).
[3] S. Frank, P. Poncharal, Z. L. Wang, and W. A. de Heer, Science **280**, 1744 (1998).
[4] R. Saito, R. Matsuo, T. Kimura, G. Dresselhaus, and M. S. Dresselhaus, Chem. Phys. Lett. **348**, 187 (2001).
[5] M. H. Park, J. W. Jang, C. E. Lee, and C. J. Lee, Appl. Phys. Lett. **86**, 023110 (2005).
[6] T. Sugai, H. Yoshida, T. Okazaki, and H. Shinohara, Nano Lett. **3**, 769 (2003).
[7] M. Abe, H. Kataura, H. Kira, T. Kodama, S. Suzuki, Y. Achiba, K.-I. Kato, M. Takata, A. Fujiwara, K. Matsuda, and Y. Maniwa, Phys. Rev. B **68**, 041405(R) (2003).
[8] J. Wei, B. Jiang, X. Zhang, H. Zhu, and D. Wu, Chem. Phys. Lett. **376**, 753 (2003).
[9] R. M. F. J. Costa, S. Friedrichs, J. Sloan, and M. L. H. Green, Carbon **42**, 2527 (2004).
[10] A. Hashimoto, K. Suenaga, K. Urita, T. Shimada, T. Sugai, S. Bandow, H. Shinohara, and S. Iijima, Phys. Rev. Lett. **94**, 045504 (2005).
[11] J. M. Zuo, I. Vartanyants, M. Gao, R. Zhang, and L. A. Nagahara, Science **300**, 1419 (2003).

[12] T. Hertel, A. Hagen, V. Talalaev, K. Arnold, F. Hennrich, M. Kappes, S. Rosenthal, J. McBride, H. Ulbricht, and E. Flahaut, Nano Lett. **5**, 511 (2005).
[13] L. C. Venema, V. Meunier, Ph. Lambin, and C. Dekker, Phys. Rev. B **61**, 2991 (2000).
[14] J. W. G. Wildoer, L. C. Venema, A. G. Rinzler, R. E. Smalley, and C. Dekker, Nature (London) **391**, 59 (1998).
[15] T. W. Odom, J. L. Huang, P. Kim, and C. M. Lieber, Nature (London) **391**, 62 (1998).
[16] R. Saito, G. Dresselhaus, and M. S. Dresselhaus, J. Appl. Phys. **73**, 494 (1993).
[17] Ph. Lambin, L. Philippe, J.-C. Charlier, and J.-P. Michenaud, Comput. Mater. Sci. **2**, 350 (1994).
[18] Y.-K. Kwon and D. Tomanek, Phys. Rev. B **58**, R16001 (1998).
[19] Y. H. Ho, C. P. Chang, F. L. Shyu, R. B. Chen, S. C. Chen, and M. F. Lin, Carbon **42**, 3159 (2004).
[20] G. W. Ho, Y. H. Ho, T. S. Li, C. P. Chang, and M. F. Lin, Carbon **44**, 2323 (2006).
[21] T. Pichler, M. Knupfer, M. S. Golden, J. Fink, A. Rinzler, and R. E. Smalley, Phys. Rev. Lett. **80**, 4729 (1998).
[22] X. Liu, T. Pichler, M. Knupfer, J. Fink, and H. Kataura, Phys. Rev. B **70**, 205405 (2004).
[23] M. F. Lin, D. S. Chuu, C. S. Huang, Y. K. Lin, and K. W.-K. Shung, Phys. Rev. B **53**, 15493 (1996).
[24] M. F. Lin and Kenneth W.-K. Shung, Phys. Rev. B **50**, 17744 (1994).
[25] M. F. Lin, D. S. Chuu, and K. W.-K. Shung, Phys. Rev. B **56**, 1430 (1997).
[26] F. L. Shyu and M. F. Lin, Phys. Rev. B **62**, 8508 (2000).
[27] C. W. Chiu, F. L. Shyu, C. P. Chang, R. B. Chen, and M. F. Lin, Phys. Lett. A **311**, 53 (2003).
[28] C. W. Chiu, C. P. Chang, F. L. Shyu, R. B. Chen, and M. F. Lin, Phys. Rev. B **67**, 165421 (2003).
[29] B. Vasvari, Phys. Rev. B **55**, 7993 (1997).
[30] C. Yannouleas, E. N. Bogachek, and U. Landman, Phys. Rev. B **50**, 7977 (1994).
[31] C. Yannouleas, E. N. Bogachek, and U. Landman, Phys. Rev. B **53**, 10225 (1996).
[32] G. Gumbs, A. Balassis, and P. Fekete, Phys. Rev. B **73**, 075411 (2006).
[33] D. J. Mowbray, Z. L. Miskovic, and F. O. Goodman, Phys. Rev. B **74**, 195435 (2006).
[34] B. Tanatar, Phys. Rev. B **55**, 1361 (1997).
[35] A. M. Lunde, K. Flensberg, and A.-P. Jauho, Phys. Rev. B **71**, 125408 (2005).
[36] M. F. Lin and Kenneth W.-K. Shung, Phys. Rev. B **47**, 6617 (1993).
[37] S. Roche, F. Triozon, A. Rubio, and D. Mayou, Phys. Rev. B **64**, 121401(R) (2001).
[38] K. H. Ahn, Y. H. Kim, J. Wiersig, and K. J. Chang, Phys. Rev. Lett. **90**, 026601 (2003).
[39] J. H. Ho, C. P. Chang, and M. F. Lin, Phys. Lett. A **352**, 446 (2006).